RESEARCH PAPER

Optimizing Biocompatibility of Mg-AZ31B Alloy through Varied Surface Roughness and Anodization Time

Faraz Hussain[1], Muhammad Umar Manzoor[1], Muhammad Kamran[1], Tahir Ahmad[1], Fahad Riaz[1], Sehrish Mukhtar[1], Hafiz Muhammad Rehan Tariq[2], Muhammad Ishtiaq[1,*]

* *ishtiaq.imme@pu.edu.pk*

[1] Institute of Metallurgy & Materials Engineering, Faculty of Chemical & Materials Engineering, Quaid-e-Azam, Campus, University of the Punjab, 54590. Lahore, Pakistan

[2] Department of Mechanical Engineering, Incheon National University, Incheon, 22012, Republic of Korea

Received: July 2024 **Revised: September 2024** **Accepted: September 2024**

DOI: 10.22068/ijmse.3669

Abstract: *Magnesium alloys are increasingly valued for biomedical applications due to their biocompatibility. This study investigates Mg-AZ31B alloy samples treated with quartz and alumina grits (< 200 µm) at varied pressures, followed by anodization in an eco-friendly alkaline electrolyte. The results show that increased blasting pressure produces a rougher surface. Anodization time significantly affects the thickness of the anodic film, leading to a transition in surface morphology from fine to coarse structures with complete film coverage. Characterization by XRD reveals that the anodic film mainly comprises magnesium oxide and hydroxide phases. Open Circuit Potential (OCP) measurements demonstrate enhanced corrosion resistance post-anodization, particularly notable at 40 minutes on alumina-blasted samples. ANOVA confirms that both blasting pressure and anodization time significantly influence coating thickness and OCP, indicating the formation of a dense anodized layer.*

Keywords: *AZ31B Magnesium Alloy, Grit Blasting, Blasting Pressure, Anodization, Open Circuit Potential, Analysis of Variance (ANOVA).*

1. INTRODUCTION

Magnesium (Mg) and its alloys exhibit considerable potential for use as metallic bone fixation implants due to their inherent presence within the human body, non-toxic nature, and potential as biodegradable and biocompatible materials. Mg possesses several notable characteristics that make it a highly suitable biomaterial, such as its ability to resist fracture, low density, and high specific strength [1]. Approximately half of the Mg present in the human body is stored in bone [2], where it stimulates bone formation and enhances bone strength [3]. Mg possesses a highly attractive physical attribute in the form of its elastic modulus, which is comparable to that of human bone. Particularly, Mg has been extensively investigated as a potential bone replacement material to mitigate stress shielding, a significant factor contributing to the failure of metallic implants [4-6]. However, the primary drawback of Mg implants is their rapid degradation rates which is followed by the release of hydrogen gas and results in the creation of hydrogen gas pockets in tissues [7-9]. Moreover, Mg alloys are susceptible to significant localized corrosion, resulting in the premature decline of their mechanical strength. This poses a significant obstacle to their continued clinical utilization, particularly in cardiac and orthopedic applications [10-12].

Fortunately, multiple approaches are available to control the corrosion rates of Mg-based implants, including mechanical pre-processing, alloying, and surface modifications [4, 13-15]. Among these methods, anodization is one of the most efficient for magnesium alloys [16]. Anodization is an electrochemical process that involves the oxidation of a metal surface, resulting in the formation of an oxide film with desirable functional, aesthetic, and corrosion-resistant properties [17-21]. The treatment enhances the film's thickness, wear resistance, hardness, and biocompatibility compared to the untreated metal [19, 22]. The morphology of anodized films has been studied by several researchers. These factors include pre and post-treatments, electrical parameters, electrolyte content and treatment time. Lei et al. [23, 24] used a potentiostatic approach followed by annealing to anodize Mg alloys in concentrated 6 M and 10 M KOH solutions. The findings showed that Mg alloys with a magnesium oxide (MgO) coating were

[DOI: 10.22068/ijmse.3669]

superior in corrosion resistance to non-anodized Mg alloys. Xue et al. [21] studied the anodization process of pure Mg and Mg-AZ91D and compared their corrosion resistance by analyzing their anodization behavior with different anodization times. The results showed that the anodization process enhanced the corrosion resistance of both pure Mg and Mg-AZ91D alloy, and the anodization time significantly influenced the corrosion resistance. The corrosion resistance of anodic film was strongly associated with the temperature and current density, as demonstrated by Chai et al. [25]. The findings revealed that an anodic film with excellent corrosion resistance was obtained by applying high current density. Furthermore, the temperature of the solution adversely affected the anti-corrosion properties of the anodic film. Ximei et al. [26] investigated the formation of the anodic coating on the Mg-AZ91D alloy pretreated in an aluminum nitrate solution. The results indicated that the corrosion resistance of the Mg-AZ91D alloy was significantly improved when subjected to pretreatment in an aluminum nitrate solution, as compared to the untreated alloy. Fukuda et al. [17] studied the anodic films formed on Mg-AZ91D alloy in 3 M KOH solutions with and without 0.55 M Na_2SiO_3. The results showed that the anodic films developed with Na_2SiO_3 were thicker and more uniform compared to those without Na_2SiO_3.

Despite the large number of published works on the effects of electrolyte composition, temperature, current density and potential on the anodized coating on Mg alloys, however, the effect of surface roughness on the anodized coating on Mg alloys has not been published as far as we know. Therefore, in the current study, we study the effect of surface roughness on the coating morphology, thickness, and electrochemical behavior of anodized coating on blasted samples of AZ31B magnesium alloy.

2. EXPERIMENTAL PROCEDURES

2.1. Grit Blasting Process

Mg-AZ31B alloy samples were selected as a substrate for the grit blasting process. The grit blasting process was conducted using a pressure blasting system as outlined in our previous investigation [27]. Grit blasting was performed using abrasive particles blasted at the specimen surface at a 90-degree angle with a compressed air gun in a sealed chamber to prevent contamination from external particles and air. The blasted samples were then immersed in acetone and ultrasonically cleaned for 30 minutes to remove any surface impurities. Afterwards, the surface was wiped with a microfiber cloth and dried at 110°C for 15 minutes. The grit blasting parameters selected for this study, along with the resulting surface roughness (Ra) values measured using a Nano-Solver NT-MDT, are presented in Table 1.

2.2. Anodization Treatment

The anodization process was performed with a DC power supply (Rapid HY3005-3, 0–30V, 0–5A). The anodization treatment was carried out in an electrolyte having the composition given in Table 2. The grit-blasted AZ31B magnesium alloy samples were made the anode, while the graphite was used as the cathode. The samples were anodized at a constant voltage of 20V for 10, 20, 30, and 40 minutes at room temperature. Finally, the anodized samples were rinsed with deionized water and dried in warm air. The schematic diagram of the anodizing process is presented in Fig. 1.

Table 1. Grit Blasting Operation Parameters and Resulting Surface Roughness (Ra) Values

Abrasive Type	Abrasive Size (mesh)	Blasting Pressure (kPa)	Blasting Angle (degree)	Blasting Distance (mm)	Blasting Time (seconds)	Surface Roughness (Ra)
Alumina	<200 µm	350	90	10	20	0.035
		700	//	//	//	0.059
		1000	//	//	//	0.077
Quartz	<200 µm	350	90	10	20	0.027
		700	//	//	//	0.043
		1000	//	//	//	0.065

Table 2. Composition of Electrolyte Solution

Substance	Na_3PO_4	KOH	KF	$Al(NO_3)_3$	Na_2SiO_3	Ethylene Glycol	Deionized Water
Amount	8.197 g	42.08 g	0.15 g	1.25 g	0.075 g	125 ml	125 ml

[DOI: 10.22068/ijmse.3669]

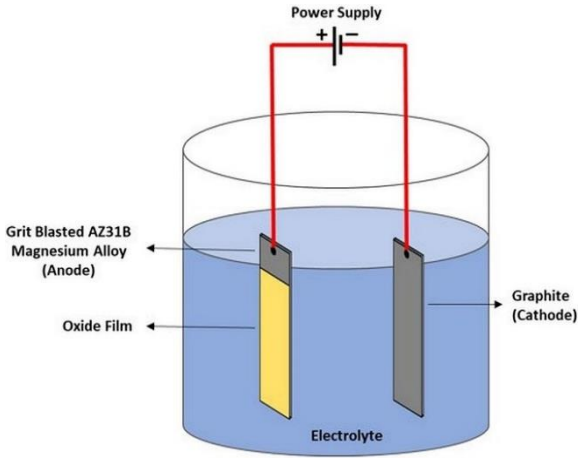

Fig. 1. Schematic diagram of the anodizing process utilized in this study

The samples were labeled as given in Table 3 to identify the process parameters under which it was processed.

2.3. Film Characterization

The surface morphology of anodized film was examined using scanning electron microscopy (SEM, FEI Inspect S50). The elemental analysis of the anodized layer was performed by an EDS system coupled with SEM consisting of a solid-state detector having a detection window of 25 mm^2. The crystal structure of the anodized layer was assessed by X-ray diffraction (XRD) analysis using a diffractometer (Equinox 2000, Thermo Scientific). Diffraction patterns were obtained using CuKα radiation (0.1546 nm) in the region of 2θ° from 10–80°. Finally, the thickness of anodized film was measured with Optical Microscopy (Leica DMI5000 M).

2.4. Electrochemical Testing

Potentiostat/Galvanostat/ZRA (Gamry Interface 1000E) was used to investigate the electrochemical behavior of anodized samples preblasted with quartz and alumina particles with different blasting pressures using open circuit potential (OCP). The electrochemical studies utilized a three-electrode system consisting of a counter electrode (graphite rod), reference electrode (Ag/AgCl saturated KCl), and working electrode. The OCP measurement was conducted for one hour. The exposed sample area was 1 cm^2. The electrolyte employed was a Ringer's lactate solution kept at 37°C.

2.5. ANOVA Analysis

Statistical analysis of the experimental results was carried out using the statistical tool Minitab 21.2 in order to establish any possible relation. The data were subjected to a two-way analysis of variance (ANOVA) with a significance level of 5% and a confidence level of 95% in order to examine the interaction, significance, and percentage contribution of input parameters to the selected responses.

3. RESULTS AND DISCUSSION

3.1. Surface Morphology

The scanning electron microscopy (SEM) micrographs of untreated and treated samples of quartz and alumina blasted AZ31B magnesium alloy are shown in Figs. 2-4, respectively.

The micrograph of the untreated pristine sample, as shown in Fig. 2(a), shows the surface scratches due to the rolling process. The micrograph of the anodizing treatment time of 10 minutes on the pristine sample is shown in Fig. 2(b), and it can be noticed that a large flake-type anodizing layer can be observed with partial coverage of the surface. However, with an increase in anodizing time from 10 to 20 minutes, the coating morphology drastically changes to a very fine structure with full surface coverage. With the increase in anodizing time from 20 to 30 and 40 minutes, the coating morphology gradually coarsened with increasing anodizing treatment time, as observed in Figs. 2(c-e) respectively.

The micrographs of the anodizing behavior of quartz-blasted samples with 350 kPa blasting pressure are shown in Figs. 3(a-e). The surface morphology of these samples shows the same trend as observed in anodized treated pristine samples.

Table 3. Labelling of Samples

Sample Labelling	Description
PS	Pristine Sample
A350, A700, A1000	Alumina blasted samples at 350, 700 and 1000 kPa
Q350, Q700, Q1000	Quartz blasted samples at 350, 700 and 1000 kPa
AT10, AT20, AT30, AT40	Anodization time of 10, 20, 30 and 40 minutes

[DOI: 10.22068/ijmse.3669]

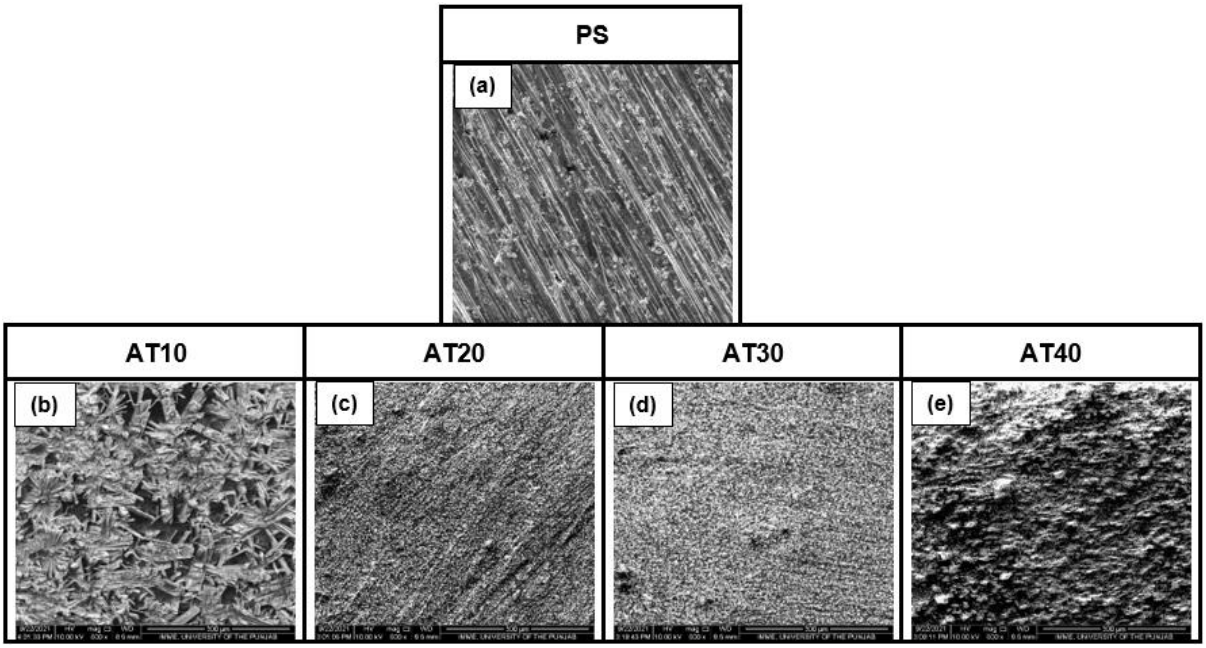

Fig. 2. SEM micrographs of pristine samples with different anodization time

The quartz-blasted samples with 700 kPa blasting pressure are shown in Figs. 3(f-j). It can be observed that the anodizing treatment at 10 minutes is quite fine and covers the whole sample. The coarsening of the anodized layer occurs with an increase in processing time to 40 minutes.

The anodizing behavior of quartz-blasted samples with 1000 kPa blasting pressure shows complete coverage for all anodizing times in Figs 3(l-o). The coarsening of the coating gradually increases with an increase in processing time. The surface morphology of the anodized surface of alumina blasted samples at different blasting pressures is shown in Fig. 4. It can be observed that the coating coverage increases with an increase in processing time. However, relative coating coverage is less for alumina-blasted samples at 350 kPa blasting pressure and increased with increased surface roughness at higher blasting pressures. From Figs. 2 and 3, it can be observed that at lower anodizing times AT10 & AT20 for pristine sample (no blasting) and for blasting at lower pressures 350 kPa i.e. lower surface roughness, the coating morphology was a flake-like structure with partial surface coverage as shown in Figs. 2(b, c) and Figs. 3(b, c) respectively. However, with increasing blasting pressure to 700kPa & 1000 kPa, the surface roughness increases, and the surface coverage also increases even at low anodizing time AT10, as shown in Figs. 3(g, l), Figs. 4(g, l). With the increase in anodizing time, pristine or blasted samples show complete coverage of the sample surface with anodized layer.

The anodized coating developed in the KOH solution resulted in a flake-type deposition on the surface as evident from Fig. 2(b) and Fig. 3(b). With an increase in deposition time, the coarse flake-type structure transforms into fine flakes as shown in Fig. 2(c), Fig. 3(c) and Fig. 3(g). With a further increase in deposition time, a thick deposited layer can be observed in all the anodized samples. The flakes continue depositing resulting in complete coverage of the surface as evident in Fig. 2(e), Figs. 3(e, j, o), and Figs. 4(e, j, o). In the quartz blasting samples, the fineness of the surface of the coating increases with an increase in surface roughness for each anodizing time as shown in Figs. 3(b, g, l), Figs. 3(c, h, m), Figs. 3(d, i, n) and Figs. 3(e, j, o). The similar trend of the surface coverage and fineness of samples blasted with alumina is much higher than that of pristine samples and quartz-blasted samples. The change in morphology and surface coverage is due to the surface roughness of blasted samples [27]. The surface roughness of the alumina-blasted samples is higher than that of the pristine sample and quartz-blasted samples. The crests and troughs on the surface create additional sites for anodization reactions, facilitating the development of anodized products. Greater surface roughness increases the reaction area, resulting

[DOI: 10.22068/ijmse.3669]

in a finer coating distribution and smaller pore sizes.

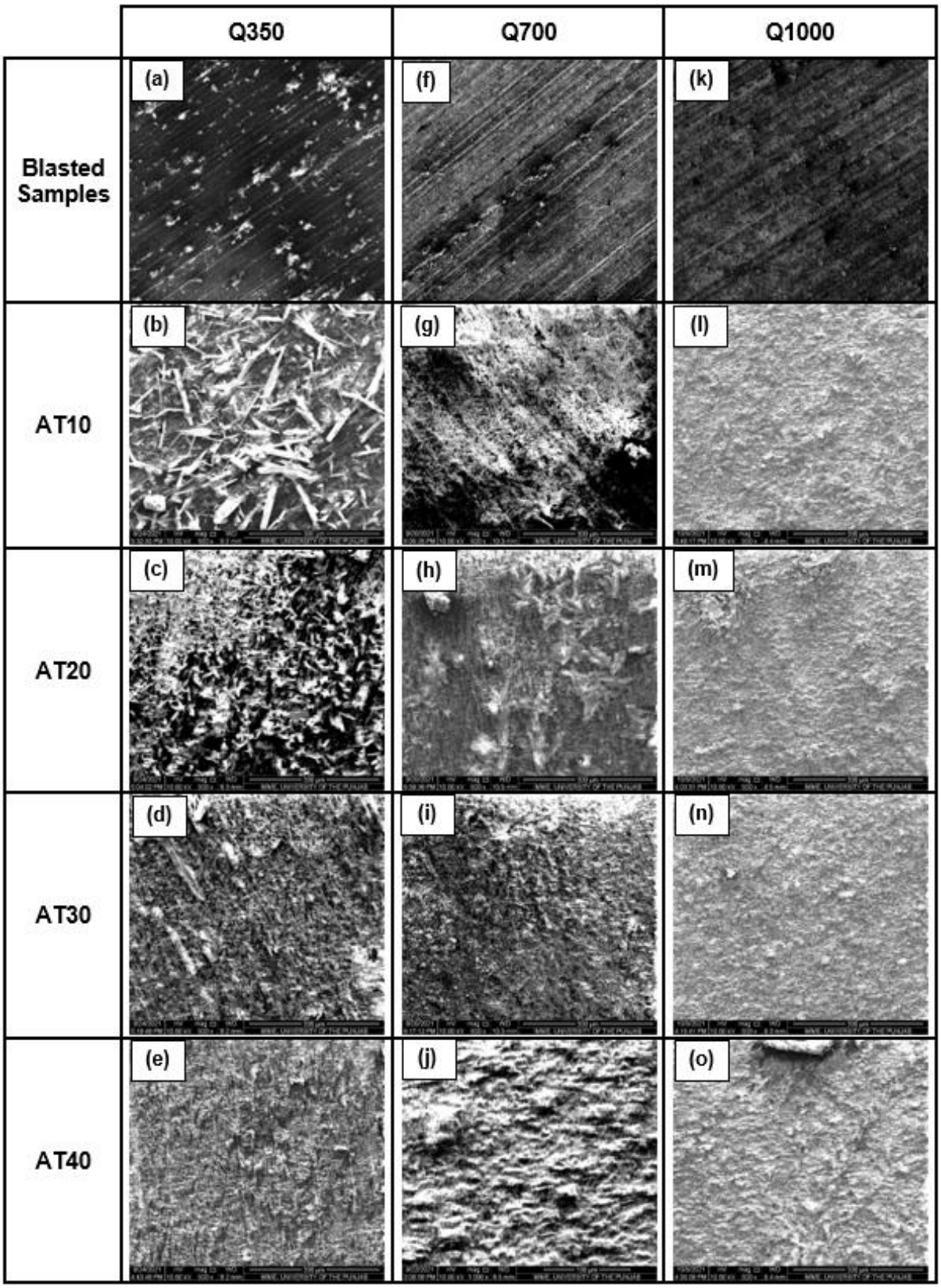

Fig. 3. SEM micrographs of quartz blasted samples with different anodization time

[DOI: 10.22068/ijmse.3669]

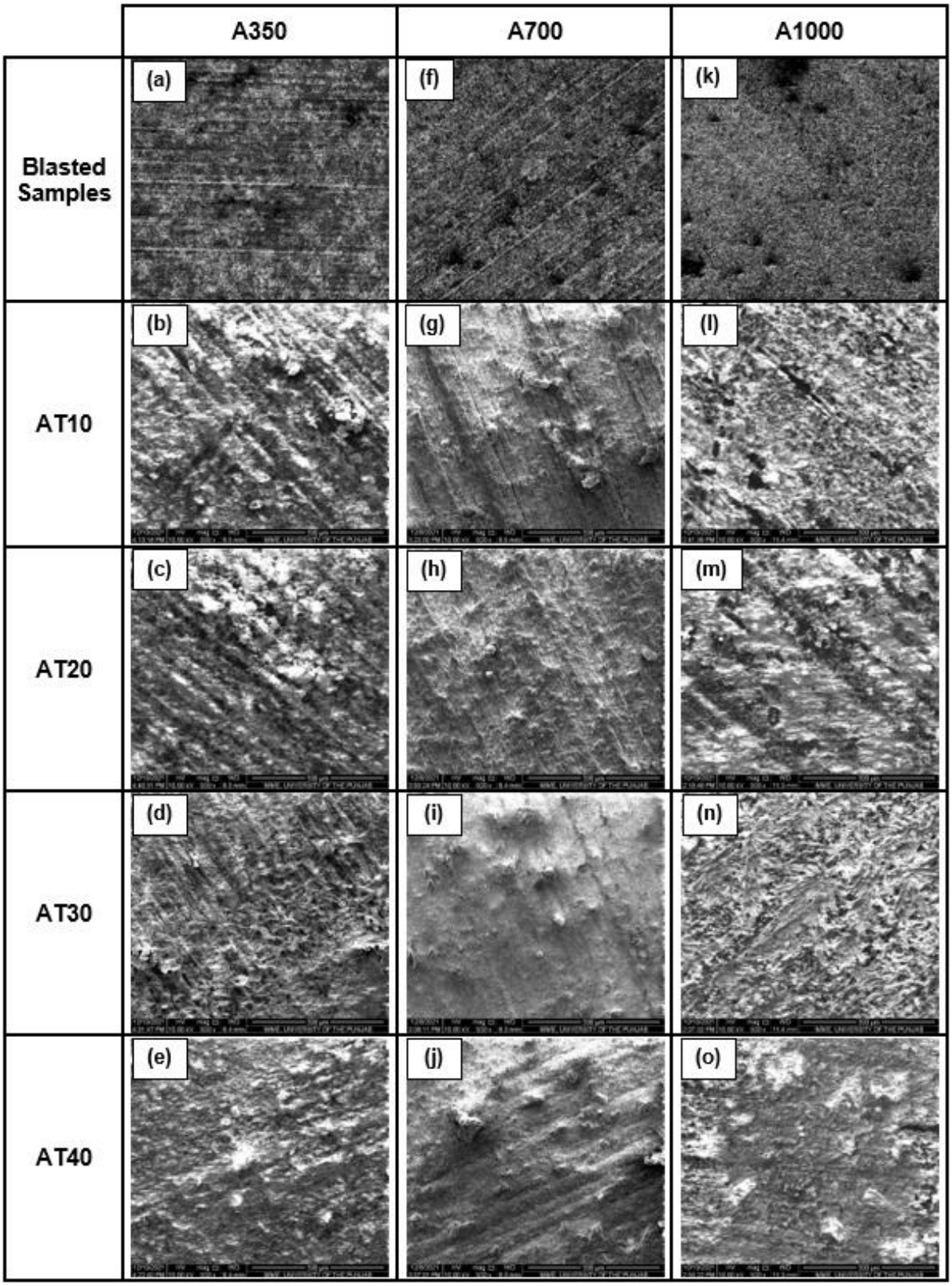

Fig. 4. SEM micrographs of alumina blasted samples with different anodization time

The high-energy surface layer of quartz and alumina blasted samples helps to increase the interaction of magnesium with solution to form an anodized layer. Anodization of magnesium is a

[DOI: 10.22068/ijmse.3669]

complex process, the anodized layer formed on the surface acts as a barrier and prevents further oxidation [28, 29]. The electrochemical reactions for anodization can be described under [30]:

$Mg = Mg^{+2} + 2e^-$ (1)

$2H_2O + 2e^- = H_2 + 2OH^-$ (2)

$Mg^{+2} + 2OH^- = Mg(OH)_2$ (3)

$Mg(OH)_2 = MgO + H_2O$ (4)

In the anodization process, the magnesium metal at the surface is converted into magnesium ions as Mg^{+2} ions (cations). The OH^- ions are produced either by H_2 evolution as given in the reaction (2) or OH^- ions available due to the hydrolyzation of KOH in the solution. The dissociated Mg^{2+} ions (cations) react with hydroxyl ions to form $Mg(OH)_2$ as given in reaction (3). At higher voltage $Mg(OH)_2$ converts to MgO and water as per reaction (4). Further, magnesium metal with OH^- ions oxidizes to form MgO at high voltage as given in reaction (5) [30].

$Mg + 2OH^- = MgO + H_2O + 2e^-$ (5)

As time passes, magnesium cations react with OH^- ions to form initially $Mg(OH)_2$ and then reduce to MgO to increase the coating thickness.

3.2. Coating Thickness Analysis

The measured anodized coating thickness values on the pristine, quartz, and alumina blasted samples after different anodization times are graphically shown in Fig. 5. It can be observed that the coating thickness increases gradually with the processing time. The regression analysis (R^2 values) confirms the linearity of the data.

The blasted samples, both with quartz and alumina, show a higher coating thickness than that of uncoated samples. The coating thickness data as shown in Figs. 5 confirms that the thickness of the anodized layer depends on the surface roughness or the nucleation sites of high energy areas created due to the surface roughness. The coating thickness of the samples blasted with alumina is higher than that of quartz-blasted samples respectively. However, as the coverage of the sample surface completes, further increase in coating thickness decreases and proceeds linearly with the increase in time. The initial exponential increase in coating thickness i.e. from 0 to 10 minutes may be due to the direct exposure of magnesium cations and magnesium metal with the OH^- ions in the solution according to reactions (3) and (5) respectively. However, the decrease in this trend i.e. from 10 to 20 minutes onward, is because of the shift, from the direct reaction of magnesium and its ions with OH^- ions due to the diffusion of magnesium cations through the developed layers to the surface to form $Mg(OH)_2$ or MgO at the interface of the anodized layer with the solution. This diffusion of magnesium cations through the deposited layer is responsible for a linear increase in coating thickness with an increase in processing time [30].

3.3. EDX Analysis

The EDX analysis of an anodized surface is shown in Fig. 6. The point analysis of a coating indicates the presence of oxygen along with magnesium and aluminum in the coating. The change in oxygen and magnesium contents of pristine samples with quartz and alumina blasted samples are graphically shown in Figs. 7.

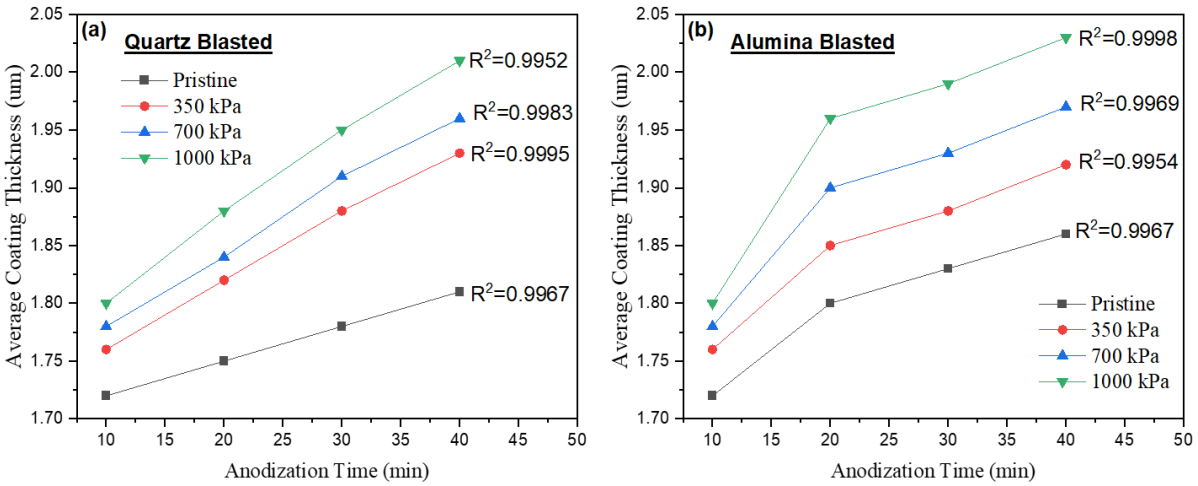

Fig. 5. Average coating thickness with increasing anodization time for pristine and (a) quartz blasted (b) alumina samples

[DOI: 10.22068/ijmse.3669]

The percentage of oxygen in the coating increases linearly with the increase in processing time. It can also be observed that oxygen and magnesium contents in the coating on the alumina blasted samples are relatively higher than that of pristine samples and quartz blasted samples for all the anodizing times. The change in increase in magnesium and oxygen contents in the EDX analysis of different anodized sample surfaces clearly shows that linear increase in the thickness of the coating.

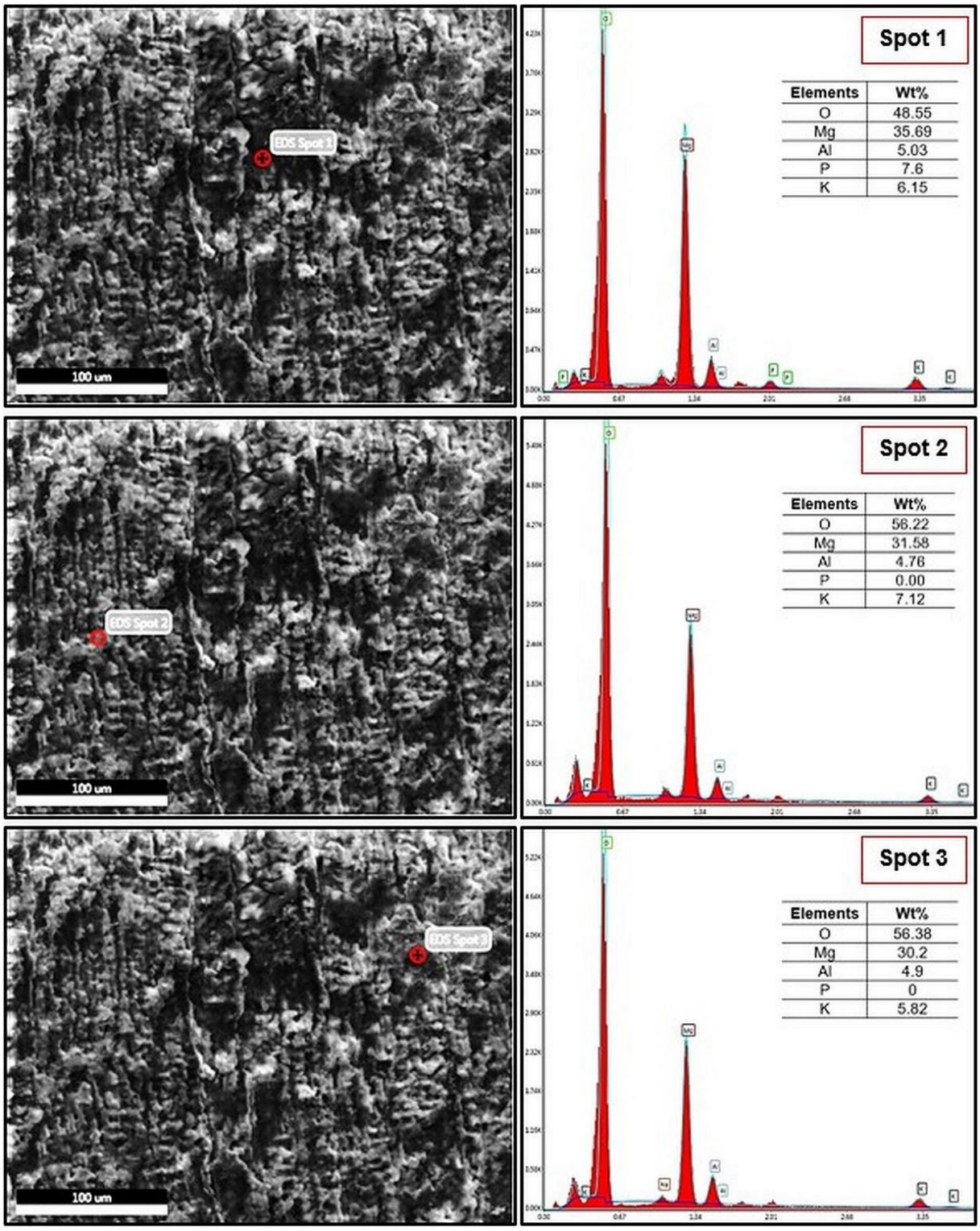

Fig. 6. EDX analysis of an anodized surface

[DOI: 10.22068/ijmse.3669]

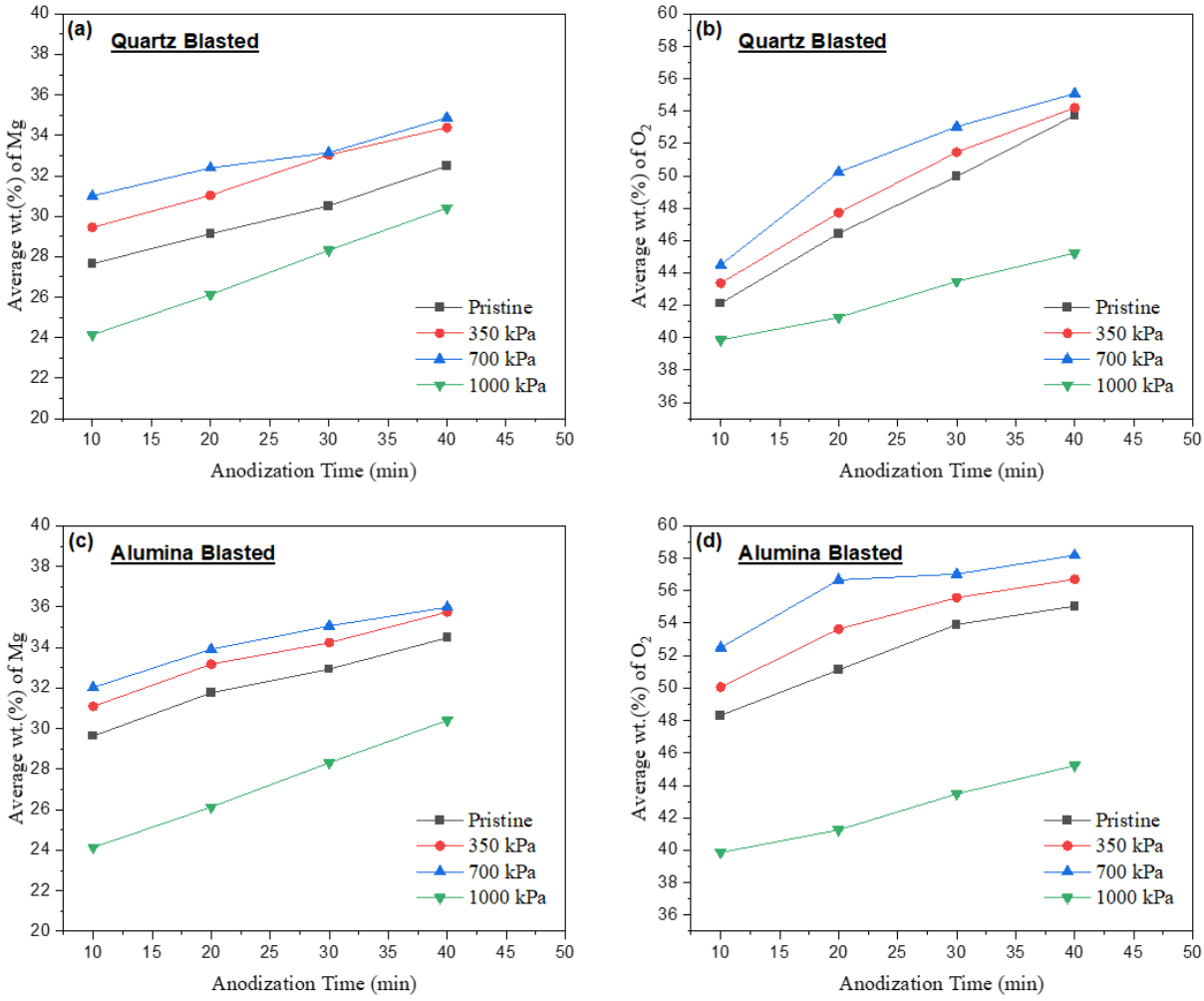

Fig. 7. Graphical representation of average weight % of (a) Mg against anodization time for pristine and quartz blasted samples (b) O_2 against anodization time for pristine and quartz blasted samples (c) Mg against anodization time for pristine and alumina blasted samples (d) O_2 against anodization time for pristine and alumina blasted samples

It has been reported in the literature that the addition of sodium silicate in KOH promotes the formation of MgO instead of $Mg(OH)_2$ and the addition of $Al(NO_3)_3$ promotes the formation of Al_2O_3 in the anodized film [31]. The EDX analysis of the coating confirms the presence of aluminum along with magnesium and oxygen.

3.4. XRD Analysis

The XRD diffractogram of an anodized surface is shown in Fig. 8. The peaks of magnesium at 32.3°, 34.4°, 36.65°, 47.8°, 68.8°, and 72.72° can be observed. Similarly, peaks at 43.04° and 62.2° confirm the presence of MgO. However, very small intensity peaks of $Mg(OH)_2$ can also be identified at 38.27°, 50.98°, 58.77° and 62.06°. Similarly, peaks of 37.7°, 43.8°, and 66.5° confirm the presence of Al_2O_3 in the coating.

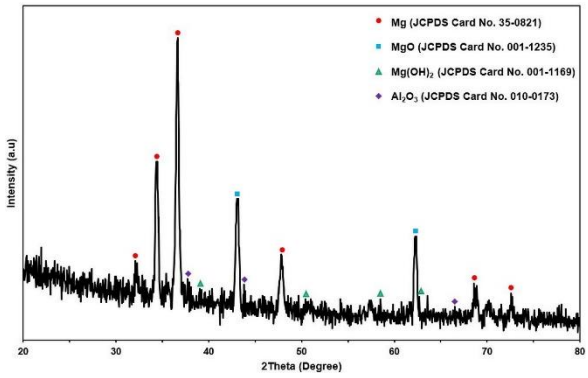

Fig. 8. XRD diffractogram of an anodized surface

The XRD diffractogram confirms the presence of MgO and Al_2O_3 in the anodized layer on the surface of the sample.

The XRD diffractogram complements the EDX analysis and the hypothesis described in the

[DOI: 10.22068/ijmse.3669]

discussion of surface morphology to support the formation of MgO in the anodized layer under the current process conditions with a very thin uppermost layer of $Mg(OH)_2$.

3.5. Open Circuit Potential (OCP)

The OCP values of pristine, quartz, and alumina blasted samples observed by anodization for different periods are graphically presented in Fig. 9. The OCP values of pristine samples anodized at different periods show the most negative values ranging from -1.684 V for 10 minutes to -1.213 V for 40 minutes confirming the poor coverage of the sample surface despite the increase in coating thickness with time. Similarly, the higher negative OCP values of the 350 kPa quartz blasted sample also confirm the porosity/incomplete coverage besides the increase in coating thickness with time. The quartz blasted sample at 700 kPa and 1000 kPa shows a drastic change from poor coverage to very good coverage when increasing the anodization time from 10 minutes to 20 minutes (about -1.5 V to about 0.5 V) and fully covered surface with thick coating for 30 minutes and 40 minutes anodizing time. On the contrary, alumina blasted samples showed approximately complete coverage with anodization time of 10 minutes at 700 kPa blasting pressure (approximately -0.5 V at 10 minutes anodizing time) and the compactness increases with increase in anodizing time with more positive values and approximately complete insulated coverage is obtained at 40 minutes anodizing time with OCP value -0.089 V for 700 kPa blasting pressure and -0.065 V for 1000 kPa blasting pressure. The OCP values represent the interaction of the exposed surface with solution/environment and thermodynamic equilibrium potential with cations/anions in Helmholtz Double Layer (HDL) and in diffusion range in solution but do not represent corrosion kinetics [32].

It has been reported in the literature that the anodized coating on magnesium is usually compact with a porous structure on the interface of the coating with the solution [33]. It has also been reported [34] that ethylene glycol-containing solution results in compact barrier-type film resulting in improved anticorrosion properties of the anodic film as can be observed in the current study.

3.6. Statistical Analysis

To quantitatively elucidate the effect of processing parameters on the anodized coating thickness, a statistical analysis in terms of Analysis of Variance (ANOVA) was conducted using the statistical software Minitab 21.2. A two-way ANOVA was performed to analyze the effect of blasting media, blasting pressure, and anodization time on coating thickness, and the results are shown in Table 4.

The two-way ANOVA results for coating thickness show a statistically highly significant interaction between blasting media and blasting pressure ($F_{(3,8)0.05}$= 15.69, P= 0.001), interaction between blasting media and anodization time ($F_{(3,8)0.05}$= 5.31, P= 0.022) and interaction between blasting pressure and anodization time ($F_{(3,8)0.05}$= 19.77, P= 0.000).

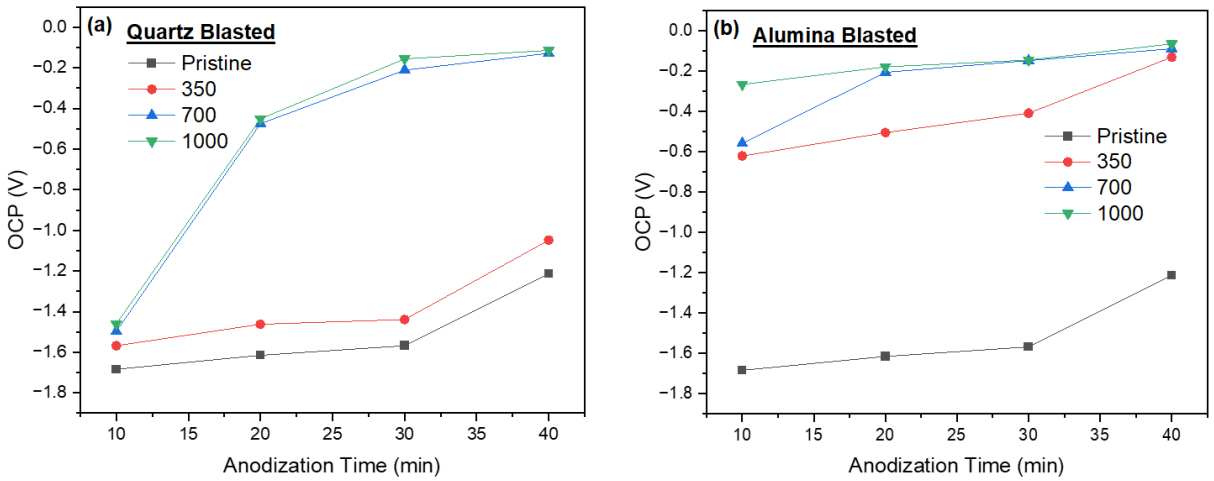

Fig. 9. Variation of OCP (v) values vs. anodization time for Pristine and (a) quartz blasted samples and (b) alumina blasted samples

[DOI: 10.22068/ijmse.3669]

Table 4. ANOVA Analysis of Coating Thickness

Source	DF	Seq SS	Contribution	Adj SS	Adj MS	F-Value	P-Value
Blasting Media	1	0.005	2.13%	0.005	0.005	138.46	0
Blasting Pressure	3	0.11585	49.31%	0.11585	0.038617	1069.38	0
Anodization Time	3	0.105075	44.72%	0.105075	0.035025	969.92	0
Blasting Media x Blasting Pressure	3	0.0017	0.72%	0.0017	0.000567	15.69	0.001
Blasting Media x Anodization Time	3	0.000575	0.24%	0.000575	0.000192	5.31	0.022
Blasting Pressure x Anodization Time	9	0.006425	2.73%	0.006425	0.000714	19.77	0
Error	9	0.000325	0.14%	0.000325	0.000036		
Total	31	0.23495	100.00%				

Statistical analysis shows that blasting pressure and anodization time are highly significant (P= 0.000) towards the coating thickness achieved during the current process contributing 49.31% and 44.72% respectively. The interaction and main effects graphs are shown in Fig. 10 and Fig. 11 respectively.

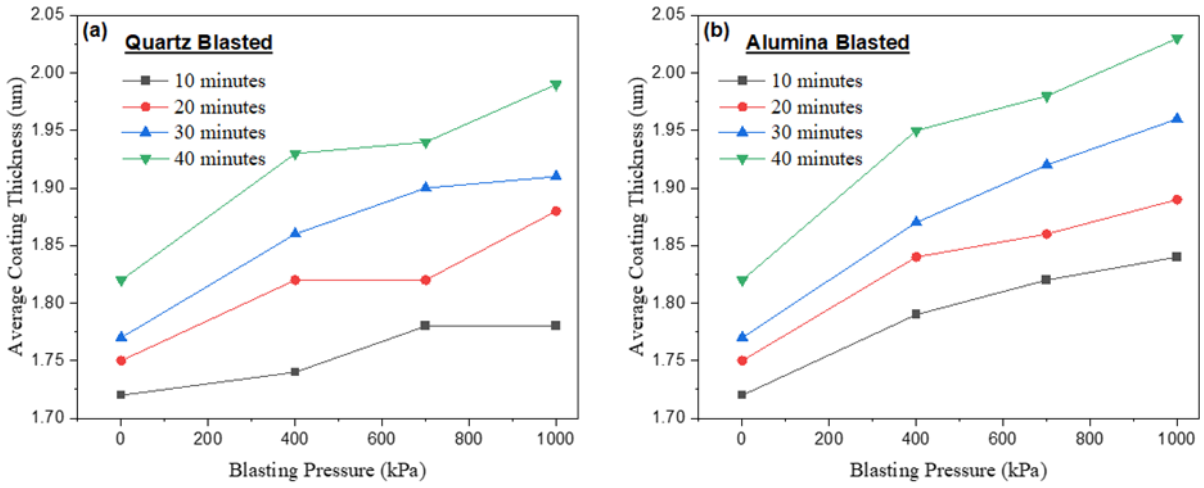

Fig. 10. Interaction plot for coating thickness

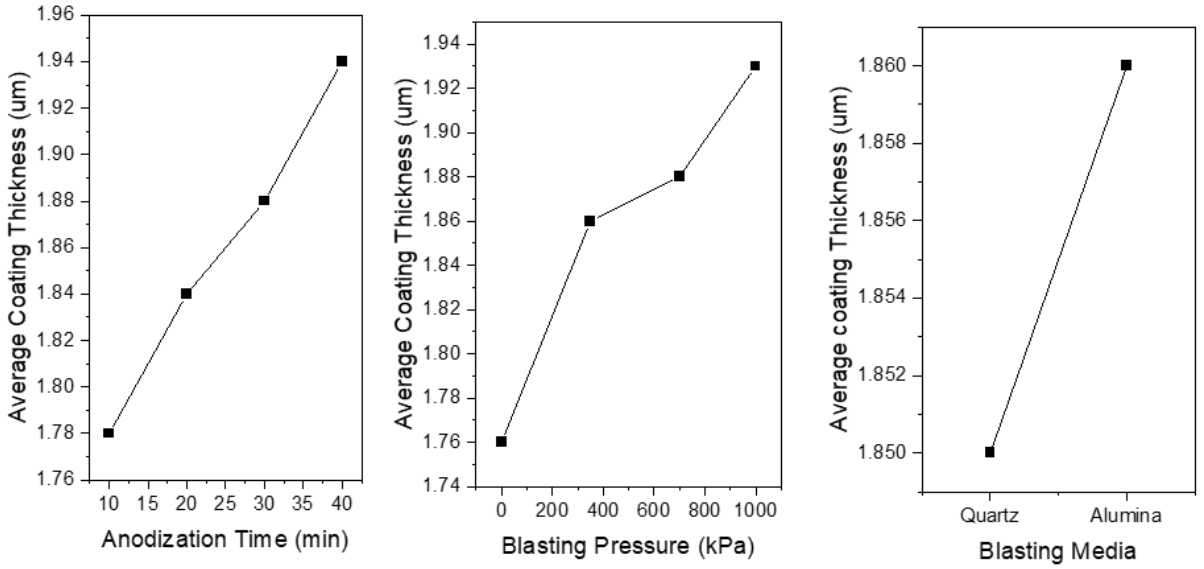

Fig. 11. Main effects plot for coating thickness

[DOI: 10.22068/ijmse.3669]

The graphs reveal that blasting pressure and anodization time have a prominent effect on the coating thickness. The results of two-way ANOVA performed to analyze the effect of blasting media, blasting pressure, and anodization time on OCP are shown in Table 5. The two-way ANOVA results for OCP show a statistically highly significant interaction between blasting media and blasting pressure (F(3,8)0.05= 7.57, P= 0.008). The two-way ANOVA results for OCP show a statistically significant interaction between blasting media and anodization time (F(3,8)0.05= 2.74, P= 0.106) and an interaction between blasting pressure and anodization time (F(3,8)0.05= 1.26, P= 0.366). Statistical analysis shows that blasting pressure is highly significant (P= 0.000) towards the OCPs achieved during the present study contributing 56.28%.

The interaction and main effects graphs are shown in Fig. 12 and 13 respectively. The graphs reveal that blasting pressure has a prominent effect on the OCP.

4. CONCLUSIONS

From the present study, the following conclusions can be drawn:

- The anodized coating thickness increased with an increase in surface roughness.
- The anodized coating thickness increased with an increase in processing time.
- The development of a flake-like coating was observed in the sodium silicate containing KOH electrolyte.
- The surface coverage increased with an increase in anodization time and increase in surface roughness i.e. maximum coverage with alumina blasted sample with 1000 kPa blasting pressure as confirmed by OCP value (-0.065V).
- The two-way ANOVA analysis of coating thickness reveals that blasting pressure and anodization mainly contributes towards coating thickness and the two-way ANOVA analysis of OCP data shows the blasting pressure is highly significant to achieve a compact anodized layer.

Table 5. ANOVA Analysis of OCP

Source	DF	Seq SS	Contribution	Adj SS	Adj MS	F-Value	P-Value
Blasting Media	1	1.3974	11.23%	1.3974	1.39737	32.99	0
Blasting Pressure	3	7.0032	56.28%	7.0032	2.3344	55.12	0
Anodization Time	3	1.8709	15.03%	1.8709	0.62364	14.72	0.001
Blasting Media x Blasting Pressure	3	0.962	7.73%	0.962	0.32067	7.57	0.008
Blasting Media x Anodization Time	3	0.3475	2.79%	0.3475	0.11584	2.74	0.106
Blasting Pressure x Anodization Time	9	0.4817	3.87%	0.4817	0.05353	1.26	0.366
Error	9	0.3812	3.06%	0.3812	0.04235		
Total	31	12.4439	100.00%				

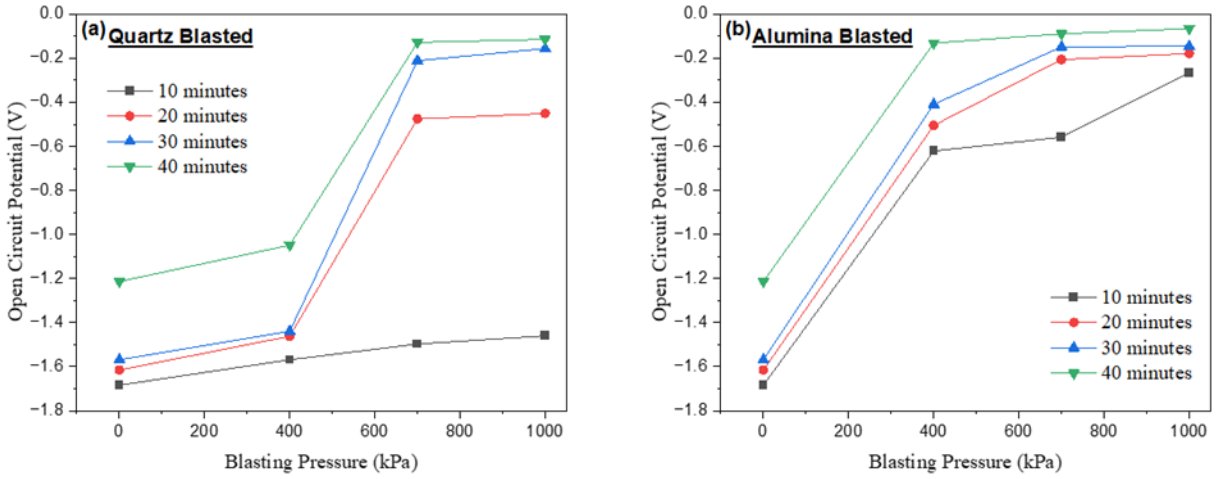

Fig. 12. Interaction plot for OCP

[DOI: 10.22068/ijmse.3669]

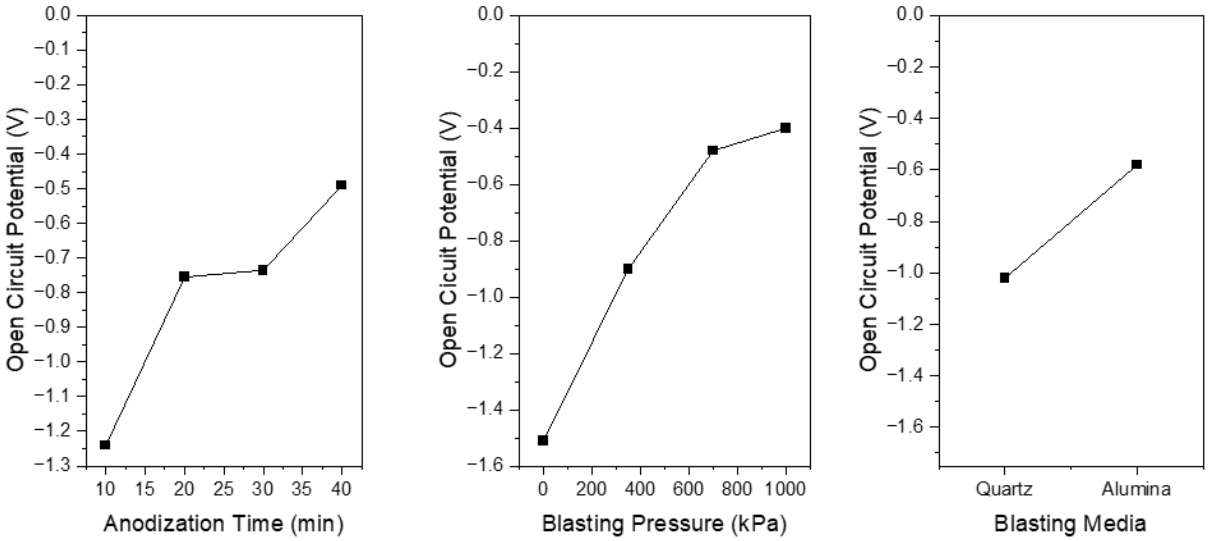

Fig. 13. Main effects plot for OCP

DATA AVAILABILITY STATEMENT

The data that support the findings of this study are available from the corresponding author upon reasonable request. All relevant data, including raw and processed data, statistical analyses, and any supplementary materials, have been stored securely and can be provided to interested researchers in compliance with institutional and ethical guidelines.

REFERENCES

[1]. Seiler, H.G. and H. Sigel, Handbook on toxicity of inorganic compounds. 1988, United States: Marcel Dekker.

[2]. Elin, R.J., Assessment of magnesium status. Clinical Chemistry, 1987. 33(11): p. 1965-1970.

[3]. Zreiqat, H., et al., Mechanisms of magnesium-stimulated adhesion of osteoblastic cells to commonly used orthopaedic implants. Journal of Biomedical Materials Research, 2002. 62(2): p. 175-184.

[4]. Staiger, M.P., et al., Magnesium and its alloys as orthopedic biomaterials: A review. Biomaterials, 2006. 27(9): p. 1728-1734.

[5]. Choi, J.-W., et al., Reinforcement of Hydroxyapatite Bioceramic by Addition of Ni_3Al and Al_2O_3. Journal of the American Ceramic Society, 1998. 81(7): p. 1743-1748.

[6]. Thamaraiselvi, T.V. and S. Rajeswari, Biological Evaluation of Bioceramic Materials -A Review. Trends in biomaterials & artificial organs, 2004. 18.

[7]. Witte, F., The history of biodegradable magnesium implants: A review. Acta Biomaterialia, 2010. 6(5): p. 1680-1692.

[8]. Witte, F., et al., In vivo corrosion of four magnesium alloys and the associated bone response. Biomaterials, 2005. 26(17): p. 3557-3563.

[9]. Kuhlmann, J., et al., Fast escape of hydrogen from gas cavities around corroding magnesium implants. Acta Biomaterialia, 2013. 9(10): p. 8714-8721.

[10]. Zhao, D., et al., Current status on clinical applications of magnesium-based orthopaedic implants: A review from clinical translational perspective. Biomaterials, 2017. 112: p. 287-302.

[11]. Kirkland, N.T., N. Birbilis, and M.P. Staiger, Assessing the corrosion of biodegradable magnesium implants: A critical review of current methodologies and their limitations. Acta Biomaterialia, 2012. 8(3): p. 925-936.

[12]. Wan, P., L. Tan, and K. Yang, Surface Modification on Biodegradable Magnesium Alloys as Orthopedic Implant Materials to Improve the Bio-adaptability: A Review. Journal of Materials Science & Technology, 2016. 32(9): p. 827-834.

[13]. Pogorielov, M., et al., Magnesium-based biodegradable alloys: Degradation, application, and alloying elements. Interventional Medicine and Applied

[DOI: 10.22068/ijmse.3669]

Science Interventional Medicine and Applied Science, 2017. 9(1): p. 27-38.
[14]. Hornberger, H., S. Virtanen, and A.R. Boccaccini, Biomedical coatings on magnesium alloys – A review. Acta Biomaterialia, 2012. 8(7): p. 2442-2455.
[15]. Hussain, F., et al., The Effect of Surface Roughness and Deposition Time on the Biocompatibility of Electrodeposited Hydroxyapatite Coating on Grit-Blasted AZ31B Mg Alloy. Iranian Journal of Science, 2024.
[16]. Shi, Z., G. Song, and A. Atrens, The corrosion performance of anodised magnesium alloys. Corrosion Science, 2006. 48(11): p. 3531-3546.
[17]. Fukuda, H. and Y. Matsumoto, Effects of Na_2SiO_3 on anodization of Mg–Al–Zn alloy in 3 M KOH solution. Corrosion Science, 2004. 46(9): p. 2135-2142.
[18]. Santamaria, M., et al., The influence of surface treatment on the anodizing of magnesium in alkaline solution. Electrochimica Acta, 2011. 56(28): p. 10533-10542.
[19]. Song, G.-L. and Z. Shi, Corrosion mechanism and evaluation of anodized magnesium alloys. Corrosion Science, 2014. 85: p. 126-140.
[20]. Blawert, C., et al., Anodizing Treatments for Magnesium Alloys and Their Effect on Corrosion Resistance in Various Environments. Advanced Engineering Materials, 2006. 8(6): p. 511-533.
[21]. Xue, D., et al., Corrosion protection of biodegradable magnesium implants using anodization. Materials Science and Engineering: C, 2011. 31(2): p. 215-223.
[22]. Song, G., Control of biodegradation of biocompatable magnesium alloys. Corrosion Science, 2007. 49(4): p. 1696-1701.
[23]. Lei, T., et al., Enhanced corrosion protection of MgO coatings on magnesium alloy deposited by an anodic electrodeposition process. Corrosion Science, 2010. 52(10): p. 3504-3508.
[24]. Lei, T., et al., Preparation of MgO coatings on magnesium alloys for corrosion protection. Surface and Coatings Technology, 2010. 204(23): p. 3798-3803.
[25]. Chai, L., et al., Anodizing of magnesium alloy AZ31 in alkaline solutions with silicate under continuous sparking. Corrosion Science, 2008. 50(12): p. 3274-3279.
[26]. Ximei, W., et al., Influence of surface pretreatment on the anodizing film of Mg alloy and the mechanism of the ultrasound during the pretreatment. Surface & Coatings Technology, 2008. 202: p. 4210-4217.
[27]. Hussain, F., et al., The Effect of Grit Blasting on Surface Roughness and Hardness of Magnesium Alloy AZ31B: A Statistical Study. Physics of Metals and Metallography, 2023. 124(13): p. 1620-1631.
[28]. K, S., et al., Titanate incorporated anodized coating on magnesium alloy for corrosion protection, antibacterial responses and osteogenic enhancement. Journal of Magnesium and Alloys, 2022. 10(4): p. 1109-1123.
[29]. Johnson, I., J. Lin, and H. Liu, Surface Modification and Coatings for Controlling the Degradation and Bioactivity of Magnesium Alloys for Medical Applications, in Orthopedic Biomaterials: Advances and Applications, B. Li and T. Webster, Editors. 2017, Springer International Publishing: Cham. p. 331-363.
[30]. Merino, E., et al., Hybrid Epoxy-Alkyl Sol–Gel Coatings Reinforced with SiO_2 Nanoparticles for Corrosion Protection of Anodized AZ31B Mg Alloy. Gels, 2022. 8(4): p. 242.
[31]. Hsiao, H.-Y., H.-C. Tsung, and W.-T. Tsai, Anodization of AZ91D magnesium alloy in silicate-containing electrolytes. Surface and Coatings Technology, 2005. 199(2): p. 127-134.
[32]. Kartsonakis, I.A., et al., Evaluation of corrosion resistance of magnesium alloy ZK10 coated with hybrid organic–inorganic film including containers. Corrosion Science, 2012. 65: p. 481-493.
[33]. Salman, S.A. and M. Okido, 8 - Anodization of magnesium (Mg) alloys to improve corrosion resistance, in Corrosion Prevention of Magnesium Alloys, G.-L. Song, Editor. 2013, Woodhead Publishing. p. 197-231.

[DOI: 10.22068/ijmse.3669]

[34]. Asoh, H. and S. Ono, Anodizing of Magnesium in Amine - Ethylene Glycol Electrolyte. Materials Science Forum - MATER SCI FORUM, 2003. 419: p. 957-962.

[DOI: 10.22068/ijmse.3669]